RETRIEVAL STUDIES IN SUPPORT OF CLOUD PROPERTY PRODUCTS FROM THE
PACE OCEAN COLOR IMAGER
Contract number: NNX15AD79G
Activities: January 9, 2016 – February 8, 2017

UW-Madison Investigators:
Steven A. Ackerman (PI)
R. Frey
A. Heidinger
R. Holz
A. Walther

Table of Contents

Contents

List of Figures

Introduction

The team will study the retrieval capability of an OCI/A-like instrument, including data product quality relative to MODIS and VIIRS cloud data records, with the goal of understanding the ability of a PACE imager to continue and/or complement the existing imager products. We will use a combination of theoretical and empirical (satellite and field campaign datasets) approaches. The UW-Madison team is focused on development and assessment of algorithms for cloud masking and cloud height determination. This report summarizes results for the 2nd year of this work.

Cloud Mask Algorithm

A possible model to follow in the construction of an OCI cloud detection system would be the 1km MODIS Cloud Mask (MOD35) that combines several spectral cloudy and clear sky detection tests. Many pixels are partially cloudy or contain sub-pixel sized clouds. Also, clear vs. cloudy radiance-based thresholds are typically not constant over the globe but are functions of solar and view angles, ecosystem types, and season, among others. Given these realities, the MODIS mask uses a "fuzzy logic" approach where spectral cloud test results are defined as a "confidence of clear sky", with values ranging from 1.0 (confident clear) to 0.0 (confident cloudy) that correspond to a threshold range for each test. The confidences are then combined to form a preliminary clear/cloud decision. Pixel radiances are then further subjected to a stringent set of clear sky spectral tests to get the final result, one of four possibilities: confident clear, probably clear, probably cloudy, and confident cloudy.

Year 2 saw the creation of a new code and algorithm base for the OCI cloud mask built on successful heritage methods, most notably, the MODIS cloud mask (MYD35) and the MODIS-VIIRS cloud mask (MVCM). The MYD35 employs as many MODIS spectral channels as possible (Ackerman et al., 1998, Frey et al, 2008), while the MVCM only uses those spectral channels common to both MODIS and VIIRS. The table shows comparisons between the MODIS Aqua cloud mask, MVCM using MODIS Aqua data as input, and the MVCM using NPP VIIRS data as input, where CALIOP lidar cloud detection is used as a reference. Comparisons like these have become our standard method for validating cloud mask results. Hit rates for cloud detection, clear sky detection and overall ("Comb") are listed for various scene types. Hanssen-Kuiper skill scores are shown as well (Ackerman et al, 2008). As is well known, daytime ocean (rows highlighted in blue and red) is the easiest scene type for clear vs. cloudy sky discrimination. MYD35 uses 19 spectral bands in the visible, NIR, and LWIR while the MVCM uses fewer channels, only those common to both MODIS and VIIRS (Ackerman et al 2017). This decrease in available information from MYD35 to MVCM is seen in the overall hit rates where MVCM is < MYD35 by 1 %. Another decrease in accuracy is seen in the MVCM VIIRS hit rates, probably because the number and quality of collocations is not as good, as CALIOP (Winker et al 2010) and MODIS are A-train instruments and VIIRS is not. The OCI cloud mask will see a further decrease in available information via lack of LWIR bands but this can be mitigated by use of careful tuning and use of reflectance spatial variabilities. We believe the OCI mask will show similar quality when compared to lidar or other

measures of "ground truth". The next steps in OCI cloud mask development are listed under Year 3 above and will include similar comparisons to CALIOP data as shown here.

August 2014	MYD35 vs. CALIOP				MVCM Aqua vs. CALIOP				MVCM NPP vs. CALIOP (5 minute filter)			
Scene Type	HR Cloud	HR Clear	HR Comb	H-K SS	HR Cloud	HR Clear	HR Comb	H-K SS	HR Cloud	HR Clear	HR Comb	H-K SS
Global Day	91.8	88.0	90.6	79.8	93.8	81.5	89.8	75.2	90.5	81.2	87.6	71.6
60S-60N Day	91.6	90.0	91.1	81.7	94.7	82.6	90.4	77.3	92.1	81.9	88.6	74.0
Global Water	91.3	83.7	89.3	75.0	92.8	77.7	88.8	70.5	90.5	79.1	87.5	69.6
Global Water Day	94.1	84.5	**91.4**	78.6	96.8	74.6	**90.4**	71.3	92.6	75.0	**87.7**	67.6
60S-60N Water Day	93.7	86.8	**91.6**	80.5	97.3	75.7	**90.6**	73.0	94.7	75.2	**88.8**	69.9

Table 1MODIS and MODIS-VIIRS Cloud Masks vs. CALIOP Cloud Detection (Hit Rates)

A method of assessing two algorithms is to compare the results of the algorithm to the same data set. Figure 1 Here is a direct comparison between the MVCM and OCI cloud masks where both use Aqua MODIS data from August 1-7, 2014 as input. Quite similar mean cloud fractions are seen in ocean regions during this week. Currently, the OCI mask algorithm is not applied to land surfaces.

Figure 2 is the OCI minus MVCM cloud mask for the same time period as shown in Figure 1. Most differences are seen in sun-glint areas and regions characterized by large amounts of atmospheric moisture where the observations come from edge of scan. The area impacted by sun-glint will be much smaller for the OCI. So far, the OCI cloud mask is mostly just the MVCM without LWIR cloud tests. A major part of Year 3 work will be adding useful VIS/NIR spatial variability tests and re-tuning the algorithm, i.e., adjusting the relative importance of the various spectral tests, given no LWIR input data.
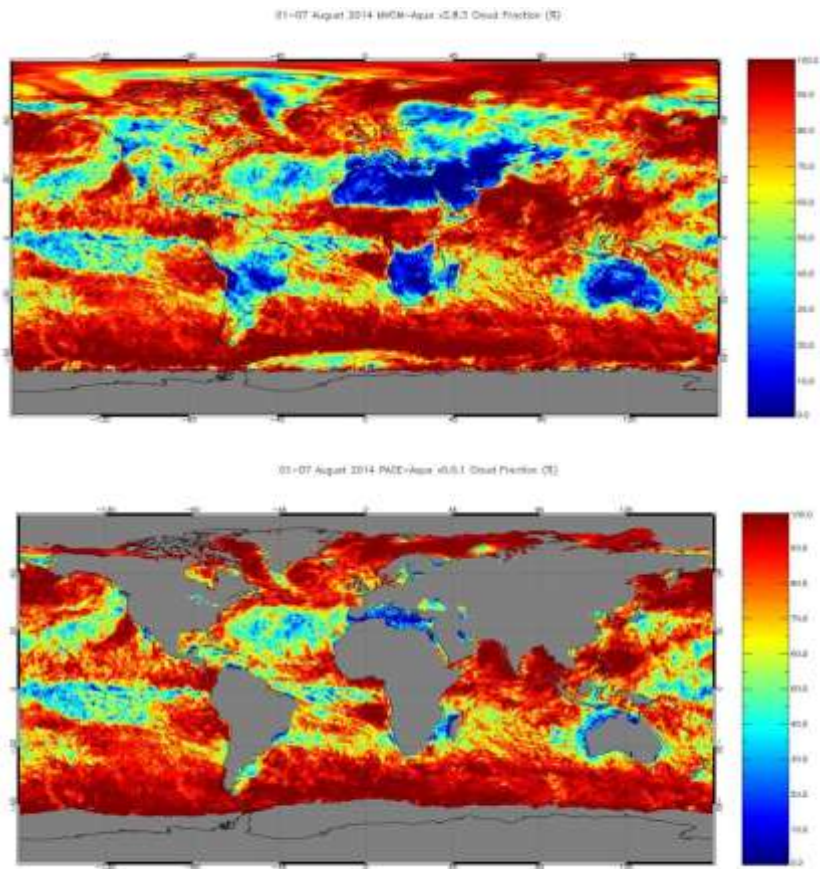
Figure 1 A direct comparison between the MVCM (top) and OCI (bottom) cloud masks where both use Aqua MODIS data from August 1-7, 2014 as input. Quite similar mean cloud fractions are seen in ocean regions during this week. The OCI algorithm is currently not executed over land and ice-covered ocean.
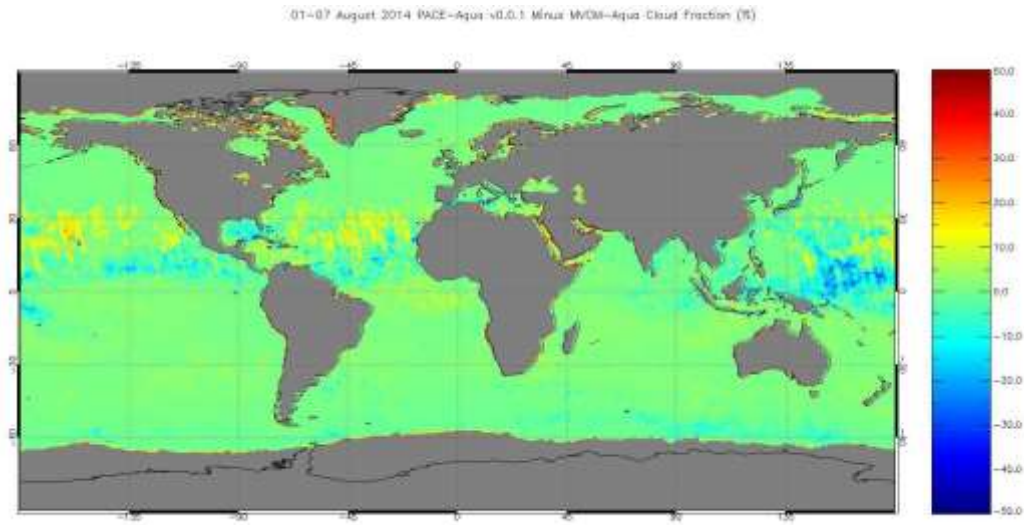
Figure 2 The OCI minus MVCM cloud mask for the same time period as shown in Figure 1.

Cloud Height Sub-Group Progress Report.

Cloud top properties

Estimates of cloud altitude using space-borne sensors have a long lineage, and most notably include the well characterized techniques using observations in thermal infrared (IR) spectral channels. Among these are the IR window techniques that provide direct estimates of cloud temperature and the CO_2 slicing technique from which cloud pressure can be estimated from the differential absorption of IR channels inside and outside the 15μm CO_2 absorption region; cloud altitude can be derived from both techniques if the atmospheric profile of temperature and pressure is known. Because OCI will not include thermal infrared channels, however, other means of estimating cloud altitude will be pursued, namely those exploiting solar spectral channels inside and outside the H_2O [e.g., Meyer et al., 2010; Wang et al., 2012] and O_2 A-band [e.g. Fischer 1991, Wang 2008] absorption regions. The sensitivity to cloud altitude of these spectral channels lies in the attenuation of the top of atmosphere (TOA) cloud reflectance due to the atmospheric gaseous absorption. Computing the ratio of the TOA reflectance of a gaseous absorbing channel to that of a window channel in close spectral proximity, coupled with knowledge of both the profile of the atmospheric gas absorber and the spectral dependence of cloud-top reflection, thus allows for estimates of cloud altitude.

Cloud altitude derived from solar absorption techniques can be notably different from that derived from IR techniques, however, a difference that results from the vertical sensitivity within the cloud of the respective spectral regimes. IR observations are sensitive to the effective level of emission within the cloud, which is near the cloud top, and the retrievals of cloud altitude tend to occur at this level. Solar reflectance measurements, on the other hand, are sensitive to the effective level of scattering which can be much deeper into the cloud than the effective level of emission, depending on the strength of the absorber, and thus retrievals of cloud altitude can be much lower in the atmosphere. Nevertheless, such solar cloud altitude retrievals, particularly the O_2 A-band

6

technique, are well understood and have been utilized on other space-borne platforms such as DSCOVR-EPIC and MERIS.

The OCI level-1 requirements include several solar spectral channels within gaseous absorption regions that can be used to estimate cloud altitude. Table 2 lists the channels relevant to the notional cloud top properties retrieval algorithm and the main absorbers.

OCI CWL (μm)	Full Width Half Maximum (nm)	Primary Absorber
0.76	5	O_2
0.86	40	window
0.94	25	H_2O
1.24	20	window
1.38	10	H_2O

Table 2 OCI spectral channels relevant to the notional cloud top properties algorithm along with the spectral widths assumed for this study.

Figure 3 provides a summary of the information content of the channels in Table 2, namely the reflectance ratio weighting functions. The weighting functions are the derivative, or slope, of the reflectance ratios with pressure, and are a function of the strength of absorption and the vertical profile of the absorber. The greater the value of the slope, the stronger the sensitivity to cloud height. The O_2 A-band ratio (0.76/0.86μm) shows moderate values throughout the atmosphere, and exhibits a linear behavior because O_2 is a uniformly mixed gas and this particular O_2 channel does not saturate (it is sensitive to low levels in the atmosphere). The 1.38/1.24μm ratio provides very high sensitivity in the upper troposphere and little information at lower levels due to the strong H_2O absorption at 1.38μm. The 0.94/0.86μm ratio, located in a less absorbing H_2O band, provides very complementary information at mid-levels in the atmosphere. Of course, the weighting functions for the 1.38 and 0.94μm ratios will vary with the moisture of the atmosphere, though for almost any atmosphere we would expect 1.38μm to provide useful information even when the surface signal at 1.38μm is not completely attenuated. Moreover, while Figure 3 implies the utility of the 0.76μm channel is negligible compared to the H_2O channels, it is important to realize that the O_2 concentration uncertainties are much lower than those of the more variable H_2O profile, and the relative contribution of the 0.76μm channel is expected to be larger than is shown here; likewise, in drier atmospheres the 0.76μm channel will be of greater importance. Given the sensitivities of the ratios in Figure 3, the notional OCI cloud-top retrievals will provide estimates of both the cloud-top pressure (P_c) and cloud pressure thickness. It is expected that these two parameters will be sufficient to capture the cloud-top information within the OCI measurements.
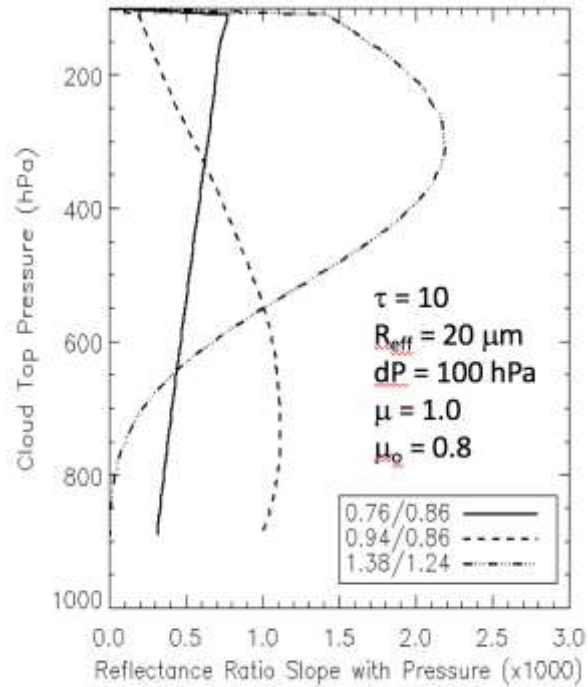
Figure 3 Clear-sky weighting functions for the OCI observations used in the notional cloud-top properties retrieval. A standard tropical atmosphere was assumed.

Radiative Transfer Modelling

To support the development of the PACE cloud top properties algorithm, the CIMSS Correlated-K (CICKER) model was modified to support the OCI channels. CICKER is based on the previously developed Successive Order of Interaction (SOI) model (Heidinger 2006). This radiative transfer model uses an adding/doubling radiative transfer solver coupled with the correlated-k method to account for atmospheric gaseous absorption. The correlated-k fitting was performed for the channels in Table 1 assuming a Gaussian spectral response function with Full width half maximum values as shown in this table. The adding/doubling solver can treat both thermal and solar sources and can handle an arbitrary number of atmospheric layers. Each layer can have water cloud, ice cloud, or aerosol (e.g., dust, smoke, volcanic ash), though only up to two cloud layers can be defined within a given profile. The cloud bulk scattering phase functions are generating by fitting Mie scattering results for liquid water clouds and severely roughened aggregate column crystals [Yang et al., 2013] for ice clouds. Mixed phase clouds can be constructed by placing ice and water clouds at the same levels. The vertical profile of effective radius within the cloud can be homogenous, vary linearly, or vary to give a constant liquid water content throughout the cloud.

A validation study of the correlated-k fits used in CICKER was performed. Table 3 shows the nadir transmission values (one-way) for the three key OCI cloud-top properties absorbing channels. The results show that CICKER adequately characterizes the gaseous absorption in each channel over a wide range of

absorber amounts. Because O_2 is a well-mixed gas, the 0.76 μm results do not change with the atmospheric profile and are a function only of the surface pressure. CICKER does show systematic transmission bias and this might be due to lack of treatment of h_2o continuum in this spectral region.

	TROPICAL		MID LAT SUM		SUB-ARCTIC SUM		SUB-ARCTIC WIN	
H_2O column	42mm		30mm		21.1mm		4.2mm	
	MOD4	CICKER	MOD4	CICKER	MOD4	CICKER	MOD4	CICKER
0.76	0.57	0.56	0.57	0.56	0.57	0.56	0.57	0.56
0.94	0.35	0.37	0.42	0.44	0.48	0.51	0.75	0.78
1.38	0.001	0.00006	0.0033	0.0006	0.48	0.51	0.135	0.125

Table 3 Nadir one-way transmission values for selected OCI bands computed for standard atmospheres from MODTRAN-4 and CICKER.

Sensitivity Analysis

To illustrate the sensitivity of the OCI channels in Table 2 to both cloud top pressure (CTP) and cloud vertical pressure thickness (CVPT), two idealized cloud cases were simulated using the CICKER radiative transfer model, namely a single layer ice cloud and a multilayer scenario of an ice cloud overlying a low-level liquid water cloud. The results of the single layer ice cloud simulations are shown in Figure 4. Panels a) to e) of **Error! Reference source not found.** show the TOA reflectance (in percent) at each of the five channels in Table 1 as a function of CTP and pressure thickness. For these two examples, we set up CICKER with the following atmospheric and observational parameters: Cloud optical thickness (COT) = 4 and effective radius = 20μm, Solar and observational zenith = 0 and 30 degrees, relative azimuth difference to 0 degrees. The atmospheric humidity profile is set to a water vapor column of 25 mm and a scale height of 2 km. Lapse rate is set to 6K/km. In the one-layer situation (Figure 4) the cloud phase is set to ice, and in the two-layer situation the lower cloud phase is set to liquid with COD of 10 and Effective radius of 13 μm between 800 and 900hPa.

The large reflectance range of the three absorbing channels (0.75, 0.94 1.38μm) is clearly evident, indicating the sensitivity of these channels to CTP and pressure thickness, while the reflectance patterns of the reference window channels (0.86, 1.24μm) are nearly uniform. Panels f) to h) show the distributions of the reflectance ratios plotted in Figure 5. While the reflectance ratio patterns indicate similar sensitivity as the absorbing channels reflectance themselves, the use of ratios is preferred since they mitigate the sensitivity to COT and microphysics relative to CTP (see Figure 4). Panel i) is a different way to visualize the values from f)- h) panels. It indicates the different sensitivities of the observable reflectance ratios to cloud top pressure for three different cloud vertical thickness values. This image gives a good impression that the sensitivity in reflectance ratios can be assumed sufficient enough for a one-layer retrieval.
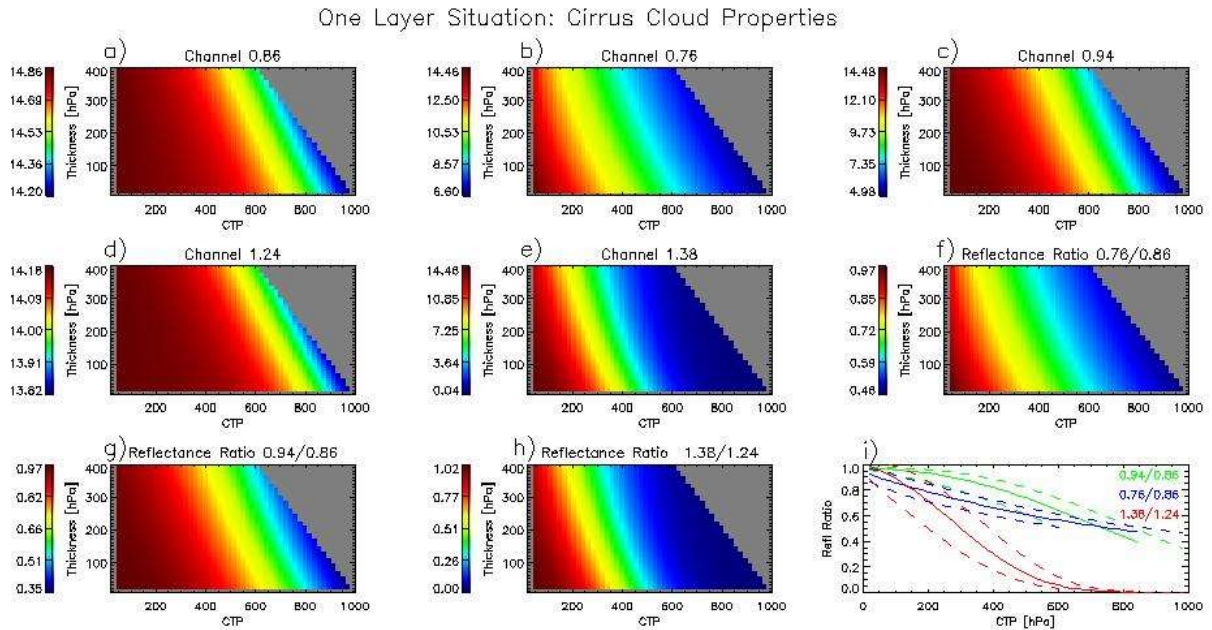
Figure 4 A sensitivity study for a single-layer ice cloud situation. The color bar values represent reflectance (in percent) for the five channels in Table 2 (Fig a-e) and reflectance ratios for three channel combinations (f-h) as a function of cloud top pressure (CTP) and cloud vertical pressure thickness. Image i) shows reflection ratio for three channel combinations as a function of CTP for a cloud thickness of 160hPa (solid line), 24hPa (dashed above solid line), and 400hPa (dashed below solid line).

Figure 5 shows the same analysis, but with an underlying low-level liquid cloud located between 800 and 900hPa with COT of 10 and effective radius of 13µm. Multi-layer situations complicate forward model and retrieval uncertainty increases in comparison to one-layer assumption. We propose to use a multi-layer detection retrieval to switch between one-layer and multi-layer (two-layer) forward models, and using a simplified assumptions of underlying cloud layer. This sensitivity study aims to illustrate that even in multilayer scenes the reflectance ratios can provide information on cloud altitude.
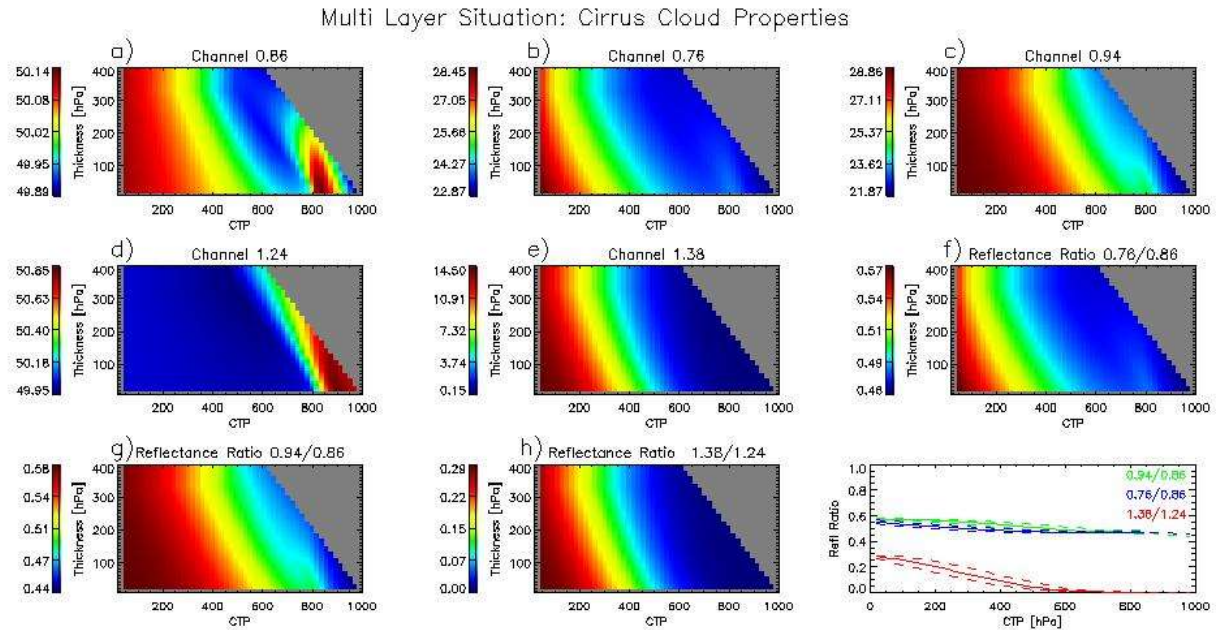
Figure 5 A sensitivity study for a multi-layer cloud scene with an assumed low-level liquid cloud between 800 and 900 HPa having optical thickness of 10 and effective radius of 13μm. The color bar values represent reflectance (in percent) for the five channels in Table 2 (Fig a-e) and reflectance ratios for three channel combinations (f-h).

Two-Channel Cloud Top Pressure Retrievals

A first-order approach to retrieving cloud altitude from absorbing solar spectral channels is to reduce the solution space to two dimensions to simultaneously infer cloud top pressure (CTP) and cloud optical thickness (COT) from the individual reflectance ratios and their respective reference channels and assuming a standard vertical thickness of the cloud. Cloud phase are assumed as known and are retrieved by preceding OCI cloud retrieval.

Example solution space for CTP for the 0.76/0.86μm (top right), 0.94/0.86μm (bottom left), and 1.38/1.24μm (bottom right) reflectance ratios versus their reference channels are shown in Figure 6; also shown is the solution space for the 0.76μm O_2 A-band absorbing channel reflectance versus the 0.86μm reference channel (top left). Here, the cloud is assumed to be vertically thin (100hPa thickness) and is placed over an ocean surface with Lambertian reflectance behavior in a tropical atmosphere. The sun is at a zenith angle of 37° and the viewing zenith is at nadir. The solid lines are constant values of cloud optical thickness and the dash-dot lines are constant cloud top pressure; note that the lower limit of each reflectance ratio is a function of the opacity of the absorbing channel. Cloud optical thickness varies from 0.25 to 128 and cloud top pressure varies from 150 to 750hPa. It is evident that the solution spaces are more orthogonal for the reflectance ratios than it is for the absorbing channel reflectance, indicating less covariance between cloud top pressure and optical thickness. However, while the optical thickness line spacing is similar for each solution space, the spacing of the constant pressure lines does show significant

variation; tighter line spacing indicates a reduced sensitivity to cloud top pressure. For the 0.76/0.86μm ratio, the pressure line spacing is relatively constant throughout the troposphere. On the other hand, the 1.38/1.24μm ratio results indicate a high sensitivity to cloud pressure in the upper troposphere but much reduced sensitivity in the lower troposphere, while the sensitivity of the 0.94/0.86μm ratio lies in the mid-levels of the troposphere. These results are consistent with the weighting functions shown in Figure 5, and demonstrate the complementary nature of the information content provided by the three reflectance ratios.
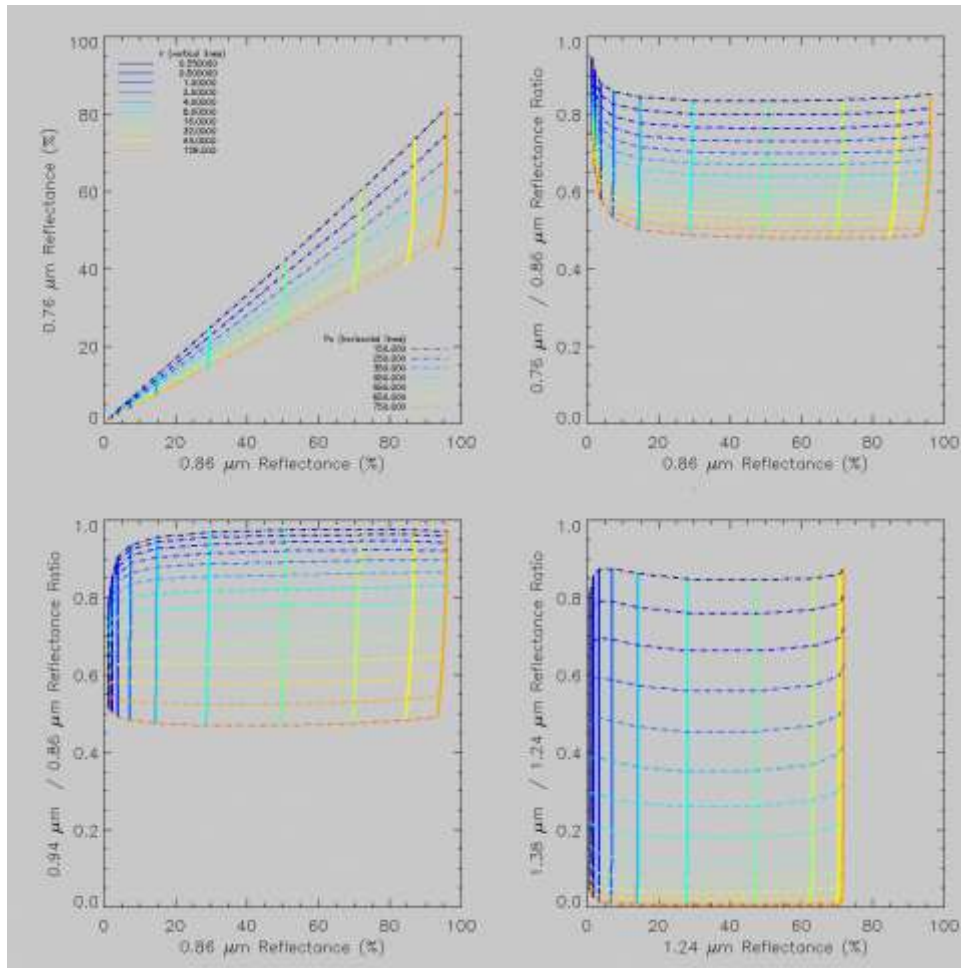
Figure 6 The variation of cloud optical depth and cloud-top pressure with the OCI absorbing channel reflectance ratios and their associated reference channel reflectance. Clouds are treated as homogenous layers with a thickness of 100 hPa, embedded in a tropical atmosphere and lying over an oceanic Lambertian surface.

Simulated retrieval errors for the reflectance ratio solution spaces in Figure 6 are shown in Figure 7. The left column of panels show the errors for a low liquid-phase cloud ($P_c = 750$ hPa) and the right column of panels show the errors for a high ice-phase cloud ($P_c = 250$ hPa); each row shows the errors from a single OCI reflectance ratio. The retrieval errors are in units of hPa for P_c and in % error for COT. The only

perturbation to the simulations was the addition of instrument noise and calibration errors. The instrument terms where added as shown:

$$R_{cont,obs} = \left(1 + {}^{\epsilon}/_{100}\right)R_{cont,true} + \delta$$

$$R_{abs,obs} = \left(1 + r_c\,{}^{\epsilon}/_{100}\right) + r_n\delta$$

Here, R_{cont} refers to window or continuum reflectance (0.86 or 1.24μm) and R_{abs} refers to the absorbing channel reflectance (0.76, 0.94 or 1.38 μm). ϵ is the calibration error taken to be 5%, and δ is the instrument noise which is assigned a value of 0.1 in reflectance units. r_c is the correlation between the calibration errors in R_{cont} and R_{abs}. For this study, r_c was set to 0.5 meaning the calibration error of the reflectance ratio is half that of the individual reflectance values. The r_n value was set to -1.0 meaning the noise is of the opposite sign on each channel, the worst case for noise cancellation. The errors and assumptions seem reasonable, but are likely too simplistic for proper OCI simulations as they are the only errors driving the values in Figure 5. Other error sources such as those from atmospheric profile, aerosol, and surface reflectance errors are ignored.

In Figure 7, the calibration error dominates the results for COT > 4, and the noise assumptions drive the results for small COT (e.g., cirrus clouds). The COT results show increased errors for thick clouds due to the non-linear relationship between reflectance and optical thickness. The cloud-top pressure results are consistent with the solution space characteristics shown in Figure 4. The CTP errors for high clouds are smallest for the 1.38/1.24μm ratio; the 0.76/0.86μm and 0.94/0.86μm ratios provide similar performance, with errors much larger than those for 1.38/1.24μm. For the low cloud, the 0.94/0.86μm results are generally superior to those of the other ratios. The 0.76/0.86μm ratio provides consistent performance for both the high and low clouds, and performs well for COT > 4 in both cases.
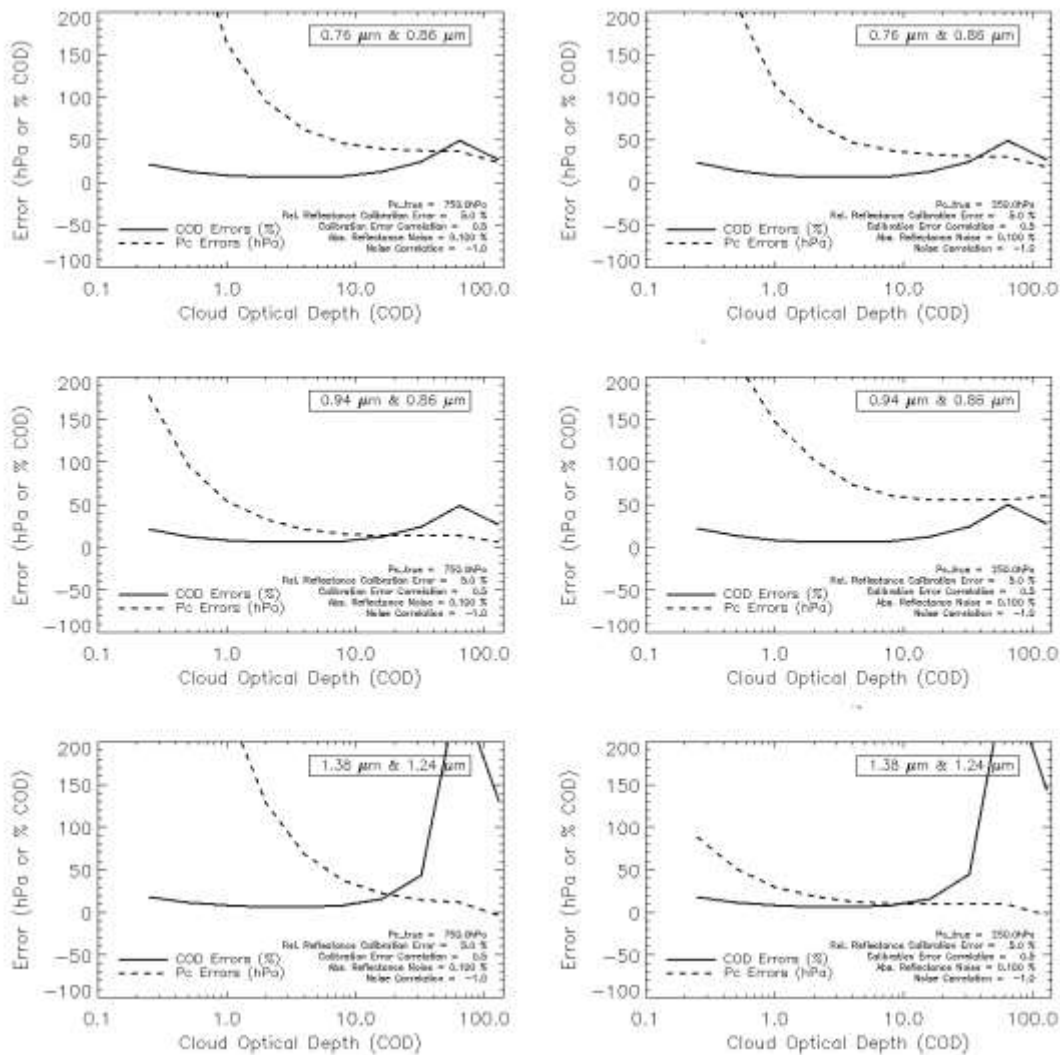
Figure 7 Simulated retrieval errors for the data in Figure 4 with an assumed calibration error of 5% and a noise of 0.1% (absolute reflectance). The panels on the left show the results as a function of optical thickness for a cloud with at 750 hPa. The panels on the right show the results as a function of optical thickness for a cloud with at 250 hPa. Errors due to atmospheric profile are ignored.

Multi-Channel Optimal Estimation Retrievals

As the previous section showed, there is significant and complementary information about cloud-top pressure in the OCI absorbing channels. The sensitivity studies showed that there is more than one piece of information on the cloud vertical structure in these measurements. The simulations in Figure 7 and Figure 8 studies showed that is sensitivity to not only the cloud-top pressure, but also the pressure thickness and the presence of multiple cloud layers.

14

To efficiently utilize the information content from all of the OCI absorbing channels simultaneously, we have developed an optimal estimation retrieval which retrieves all three products for cloud optical thickness, cloud pressure CTP, in equations also P_c) and cloud vertical pressure thickness (CVPT, in equations also Δp).

The main advantage of this approach is that it provides a convenient framework within which to add or remove spectral information from the solution. The solution is found by minimizing the difference between the observations and their estimated values derived from a forward model. The observations used in the notional OCI cloud-top retrieval are shown below as the vector y.

$$y = \begin{pmatrix} 0.86 \\ 0.76/0.86 \\ 0.94/0.86 \\ 1.38/1.24 \end{pmatrix}$$

The 0.86μm channel in this approach is included to provide sensitivity to optical thickness, and reflectance ratios are used to reduce the sensitivity of the retrieval to calibration errors. Other possible approach is to retrieve COT together with cloud effective radius (CER) in Nakajima-King retrieval scheme (Nakajima and King,1990) in advance and include COT with its uncertainty as a forward model parameter in the retrieval. In this case COT will not be optimized during the retrieval loop.
As stated above, there is more information in these measurements than a single estimate of the effective scattering level or a single cloud pressure. The errors of the forward model are the same as those used in the single channel retrievals shown in Figure 7, i.e., instrument calibration and noise. The *a priori* values for P_c are 200hPa for ice clouds and 850hPa for liquid water clouds. The Δp *a priori* values are 100hPa for all cloud phases. The *a priori* uncertainties for COT and P_c are assumed to be 20% and 500hPa, respectively and Δp *a priori* uncertainty values are 500hPa. The P_c and Δp uncertainty assume virtually no skill in the *a priori* estimate. As the retrieval matures, these assumptions will be tested and the complexities of error covariance will be studied.

Simulated OE retrieval results are shown in Figures 8-10. Note that the *a priori* values were modified from the default values for these retrievals, given the placement of the simulated clouds. Figure 6 shows a single layer ice cloud retrieval where the true cloud has optical thickness of 10, P_c = 200hPa and Δp = 100hPa. Here the *a priori* is assumed to be COT = 10, P_c = 400hPa and Δp = 50hPa. The retrieval converges after 6 iterations with P_c = 240hPa and = 60hPa.
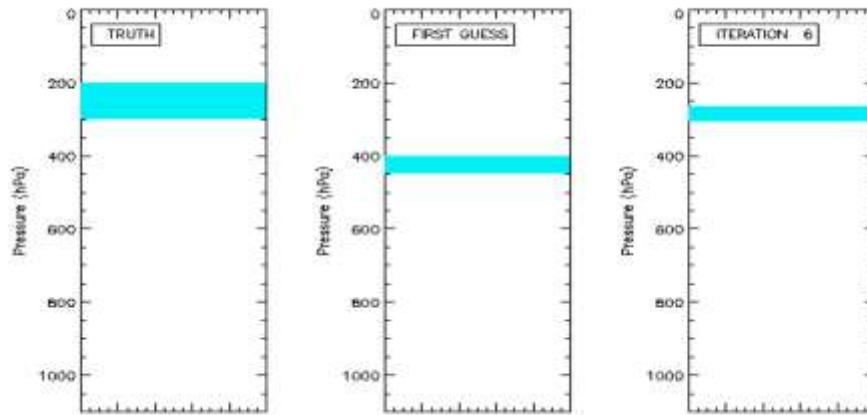
Figure 8 Simulated retrieval for a single-layer cloud with P_c = 200 hPa, Δp = 100 hPa and optical thickness = 10. The a priori settings were Pc = 400 hPa, Δp = 50 hPa and optical thickness = 10.0. The retrieval gives P_c = 260 hPa, Δp = 60 hPa and optical thickness = 10.0.

Figure 9 shows a multi-layer cloud simulation having an identical ice cloud as in Figure 8 with the addition of a lower level liquid cloud at 850hPa. Note that the retrieval still assumes a single-layer cloud in the forward model. As expected the retrieval converges on a solution that is well below the height of the higher cloud layer. These results highlight the sensitivity of these retrievals to presence of complex vertical cloud structures.

Figure 10 shows the impact of the channels used in the OE retrieval. Here, individual reflectance ratios are turned off by setting their forward uncertainty to very high values so that they have no impact on the solution. In this retrieval, the simulated cloud has P_c = 600 hPa and optical thickness = 10.0; the vertical dashed lines indicate the top and bottom of the cloud layer. The *a priori* value of P_c was 700hPa. The retrievals were performed 50 times with each retrieval having observations perturbed by random noise within the 0.1 absolute reflectance error used in Figure 7. Using only the 0.76/0.86μm ratio (red distribution), the retrieval yields P_c just above 700hPa, implying that a retrieval using only this ratio cannot improve much on the *a priori*, at least for this scenario. Including the 0.96/0.86μm ratio that was shown to be sensitive to clouds in the middle troposphere greatly improves the accuracy of the retrieval, yielding P_c centered around 620hPa (blue distribution). The accuracy is improved further with the addition of the 1.38/1.24μm ratio (green distribution).
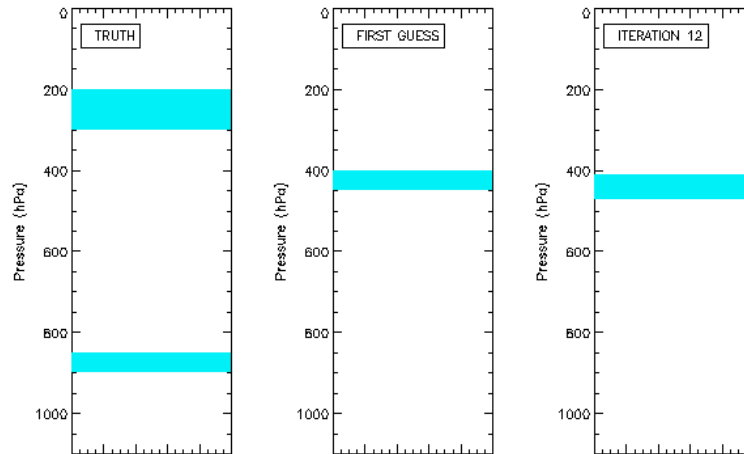
Figure 9 Same ice cloud as shown in Figure 8 but with a lower level liquid cloud with optical thickness of 10 inserted below. The single-layer retrieval assumption results in a retrieval solution below the higher cloud with optical thickness equal to the combined optical thickness of the two clouds.
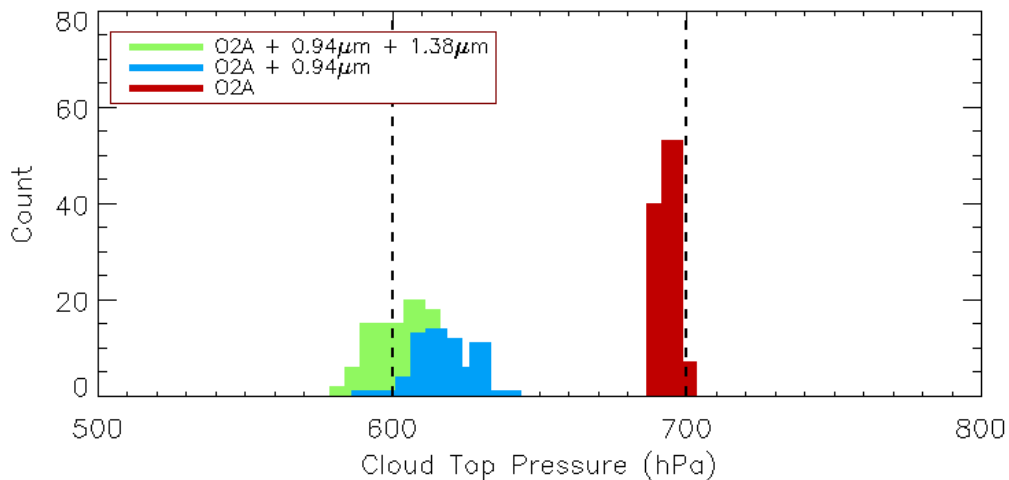
Figure 10 Simulated retrieval performance for a single-layer cloud with optical thickness of 10 and Δp of 100 hPa. The true P_c is 600hPa and the a priori value is 700hPa.

The above OE retrieval simulations do indicate that there is benefit from combing multiple channels together. In these experiments, we allowed cloud pressure height and thickness to capture the information on cloud vertical structure. Work continues on verifying that choice of these two variables is optimal. For example, the vertical structure could also be treated as profile of optical depth in discrete layers or as simplified multi-layer situations as published in (Watts et al. 2011)

References

Ackerman, S. A., K. I. Strabala, W. P. Menzel, R. A. Frey, C. C. Moeller, and L. E. Gumley Discriminating Clear-sky from Clouds with MODIS, 1998: *J. Geophys. Res.*, **103**, D24, 32,141

Ackerman, S. A., R. E. Holz, R. Frey, E. W. Eloranta, B. Maddux, and M. McGill, 2008: Cloud Detection with MODIS: Part II Validation, *J. Atmos. Oceanic Tech.*, **25**, 1073-1086.

Ackerman, S. A., R. A. Frey, R. E. Holz, S. Platnick, and A. Heidinger, 2017: Progress Towards MODIS and VIIRS Cloud Fraction Data Record Continuity. 97th Annual meeting of the American Meteorological Society, Seattle, WA, January 22 - 26

Fischer, J.; Grassl, H. Detection of cloud-top height from backscattered radiances within the Oxygen A Band. Part 1: Theoretical study. J. Appl. Meteor **1991**, 30, 1245–1259.

Frey, R. A., S. A. Ackerman, Y. Liu, K. I. Strabala, H. Zhang, J. Key and X. Wang, 2008: Cloud Detection with MODIS, Part I: Recent Improvements in the MODIS Cloud Mask, *J. Atmos. Oceanic Tech.,* **25**, 1057-1072.

Heidinger, A. K., C. O'Dell, R. Bennartz, and T. Greenwald (2006): The successive-order-of-interaction radiative transfer model. Part I: Model development. J. Appl. Meteor. and Clim., 45, 1388-1402.

Meyer, K., and S. Platnick (2010), Utilizing the MODIS 1.38 μm channel for cirrus cloud optical thickness retrievals: Algorithm and retrieval uncertainties, J. Geophys. Res., 115, D24209, doi:10.1029/2010JD014872.

Nakajima, T., and M. D. King, 1990: Determination of the optical thickness and effective particle radius of clouds from reflected solar radiation measurements. Part I: Theory. *J. Atmos. Sci.*, **47**, 1878–1893

Wang, P., Stammes, P., van der A, R., Pinardi, G., and van Roozendael, M.: FRESCO+: an improved O_2 A-band cloud retrieval algorithm for tropospheric trace gas retrievals, Atmos. Chem. Phys., 8, 6565-6576, doi:10.5194/acp-8-6565-2008, 2008.

Wang, C., S. Ding, P. Yang, B. Baum, and A. E. Dessler (2012), A new approach to retrieving cirrus cloud height with a combination of MODIS 1.24- and 1.38-μm channels, Geophys. Res. Lett., 39, L24806, doi:10.1029/2012GL053854.

Watts, P., R. Bennartz, and F. Fell, 2011: Retrieval of two-layer cloud properties from multi-spectral observations using optimal estimation, J. Geophys. Res. doi:10.1029/2011JD015883.

Winker, D. M., J. Pelon, J. A. Coakley, Jr., S. A. Ackerman, R. J. Charlson, P. R. Colarco, P. Flamant, Q. Fu, R. Hoff, C. Kittaka, T. L. Kubar, H. LeTreut, M. P. McCormick, G. Megie, L. Poole, K. Powell, C. Trepte, M. A. Vaughan, and B. A. Wielicki, 2010: The CALIPSO Mission: A Global 3D View of Aerosols and Clouds. *Bull. Amer. Met. Soc*. **91**, no.9, 2010, pp1211-1229.